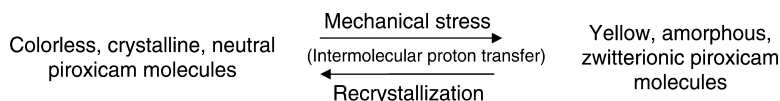Article

Mechanochromism of Piroxicam Accompanied by Intermolecular Proton Transfer Probed by Spectroscopic Methods and Solid-Phase Changes

Agam R. Sheth, Joseph W. Lubach, Eric J. Munson, Francis X. Muller, and David J. W. Grant

Colorless, crystalline, neutral piroxicam molecules
→ Mechanical stress (Intermolecular proton transfer)
← Recrystallization
Yellow, amorphous, zwitterionic piroxicam molecules

More About This Article

Additional resources and features associated with this article are available within the HTML version:

- Supporting Information
- Links to the 3 articles that cite this article, as of the time of this article download
- Access to high resolution figures
- Links to articles and content related to this article
- Copyright permission to reproduce figures and/or text from this article

View the Full Text HTML

Mechanochromism of Piroxicam Accompanied by Intermolecular Proton Transfer Probed by Spectroscopic Methods and Solid-Phase Changes

Agam R. Sheth,[†] Joseph W. Lubach,[‡] Eric J. Munson,[‡] Francis X. Muller,[§] and David J. W. Grant*,[†]

Contribution from the Department of Pharmaceutics, College of Pharmacy, University of Minnesota, Weaver-Densford Hall, 308 Harvard Street SE, Minneapolis, Minnesota 55455-0343, Department of Pharmaceutical Chemistry, The University of Kansas, 2095 Constant Avenue, Lawrence, Kansas 66047, and GlaxoSmithKline Pharmaceuticals, P.O. Box 1539, 709 Swedeland Road, King of Prussia, Pennsylvania 19406-0939

Received July 12, 2004; E-mail: grant001@umn.edu

Abstract: Structural and solid-state changes of piroxicam in its crystalline form under mechanical stress were investigated using cryogenic grinding, powder X-ray diffractometry, diffuse-reflectance solid-state ultraviolet−visible spectroscopy, variable-temperature solid-state ^{13}C nuclear magnetic resonance spectroscopy, and solid-state diffuse-reflectance infrared Fourier transform spectroscopy. Crystalline piroxicam anhydrate exists as colorless single crystals irrespective of the polymorphic form and contains neutral piroxicam molecules. Under mechanical stress, these crystals become yellow amorphous piroxicam, which has a strong propensity to recrystallize to a colorless crystalline phase. The yellow color of amorphous piroxicam is attributed to charged piroxicam molecules. Variable-temperature solid-state ^{13}C NMR spectroscopy indicates that most of the amorphous piroxicam consists of neutral piroxicam molecules; the charged species comprise only about 8% of the amorphous phase. This ability to quantify the fractions of charged and neutral molecules of piroxicam in the amorphous phase highlights the unique capability of solid-state NMR to quantify mixtures in the absence of standards. Other compounds of piroxicam, which are yellow, are known to contain zwitterionic piroxicam molecules. The present work describes a system in which proton transfer accompanies both solid-state disorder and a change in color induced by mechanical stress, a phenomenon which may be termed mechanochromism of piroxicam.

Introduction

Tautomerism in the solid-state often involves proton transfer. Solid-state proton transfers occur in many chemical and biological processes and have long been a subject of experimental study and theoretical interest. In nonpolymeric, single-component, organic molecular crystals, such proton transfers can be either dynamic or induced by external stimuli. Dynamic proton tautomerism occurs in porphyrins,[1] azophenins,[2] pyrazoles,[3] dimethyldibenzotetraaza[14]annulene,[4] citrinin,[5] and crystalline and amorphous phthalocyanine.[67] When proton transfer is induced by external stimuli, the tautomeric change is sometimes accompanied by a change in color. 4-Oxopyrimidine is an example of phototautomerism, which implies that intramolecular proton transfer is induced by ultraviolet light.[6] However, no color change accompanies the tautomeric change.[6] Proton-transfer reactions induced by external stimuli can also be accompanied by a reversible change in color, which is denoted by the suffix -*chromism*.[7] The prefix before chromism indicates the phenomenon that induces the change, on which the position and intensity of electronic bands depend. The term *chromism* originally indicated a reversible color change, but is now sometimes employed in a broader sense[8] to include irreversible color changes.[9] In general, several different types of chromisms have been defined[7] and reported, such as photochromism,[7] electrochromism,[10,11] thermochromism,[12] piezochromism,[13] tribochromism[14] solvatochromism,[11] affi-

† University of Minnesota.
‡ The University of Kansas.
§ GlaxoSmithKline Pharmaceuticals.
(1) Limbach, H. H.; Hennig, J.; Kendrick, R.; Yannoni, C. S. *J. Am. Chem. Soc.* **1984**, *106*, 4059−4060. Frydman, L.; Olivieri, A. C.; Diaz, L. E.; Frydman, B.; Morin, F.; Mayne, C. L.; Grant, D. M.; Adler, A. *J. Am. Chem. Soc.* **1988**, *110*, 336; Frydman, L.; Olivieri, A. C.; Diaz, L. E.; Vega, S.; Kustanovic, I.; Frydman, B. *J. Am. Chem. Soc.* **1989** *111*, 7001. Braun, J.; Schlabach, M.; Wehrle, B.; Matthias, K.; Vogel, E.; Limbach, H. H. *J. Am. Chem. Soc.* **1994**, *116*, 6593−6604.
(2) Rumpel, H.; Limbach, H. H. *J. Am. Chem. Soc.* **1989**, *111*, 5429−5441.
(3) Aguilar-Parilla, F.; Scherer, G.; Limbach, H. H.; Foces-Foces, M.; Cano, F. H.; Smith, J. A. S.; Toiron, C.; Elguero, J. *J. Am. Chem. Soc.* **1992**, *114*, 9657−9659.
(4) Hoelger, C.-G.; Wehrle, B.; Benedict, H.; Limbach, H. H. *J. Phys. Chem.* **1994**, *98*, 843−851.
(5) Destro, R. *Chem. Phys. Lett.* **1991**, *181*, 232−236.
(6) Nowak, M. J.; Fulara, J.; Lapinski, L. *J. Mol. Struct.* **1988**, *175*, 91−96.

(7) Bouas-Laurent, H.; Durr, H. *Pure Appl. Chem.* **2001**, *73*, 639−665.
(8) Carpick, R. W.; Sasaki, D. Y.; Burns, A. R. *Langmuir* **2000**, *16*, 1270−1278.
(9) Muller, H.; Eckhardt, C. J. *Mol. Cryst. Liq. Cryst.* **1978**, *45*, 313.
(10) Monk, P. M. S.; Mortimer, R. J.; Rosseinsky, D. R. *Electrochromism: Fundamentals and Applications*; VCH: Weinheim, Germany, 1995.
(11) Liptay, W. *Angew. Chem., Int. Ed. Engl.* **1969**, *8*, 177−188.
(12) Ault, A.; Kopet, R.; Serianz, A. *J. Chem. Educ.* **1971**, *48*, 410.
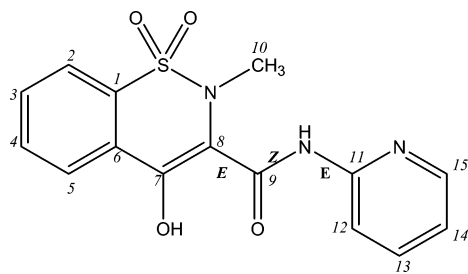(13) Schonberg, A.; Elkaschef, M.; Nosseir, M.; Sidky, M. M. *J. Am. Chem. Soc.* **1958**, *80*, 6312−6315.

Figure 1. Molecular structure of piroxicam, 4-hydroxy-2-methyl-*N*-2-pyridinyl-2*H*-1,2-benzothiazine-3-carboxamide. The piroxicam molecule in polymorph I (**P$_I$**) and polymorph II (**P$_{II}$**)[29,30] is found to exist in a near-planar *EZE* configuration about the three bonds connecting the two ring systems shown above.[32] The numbering of the carbon atoms in the above structure corresponds to that in Figures 5 and 6 for the variable-temperature ^{13}C solid-state nuclear magnetic resonance spectra.

nochromism or biochromism,[15−17] heliochromism,[18] and halosolvatochromism.[19] The term *mechanochromism* has been used to indicate that the color change is initiated by mechanical stress.[8,20,21] Terms such as reversible[22,23] and irreversible mechanochromism[9] are also used. In accordance with the IUPAC definition of chromism,[7] the present work refers to mechanochromism as a reversible color change due to mechanical stress. Few examples of color change due to proton transfer induced by external stimuli have been reported in nonpolymeric, single-component, organic molecular solids. Because these chromisms involve proton transfer, the reactants and products are tautomers. Examples include photochromism of 2-(2′,4′-dinitrobenzyl)-pyridine,[24] photo- and thermochromism of the crystal forms of *N*-salicylideneanilides,[25] and thermochromism of the 4,4′-dipyridinium salt of squaric acid.[26] Thermal tautomerism and thermochromism in salicylidene anilide derivatives have also been studied at cryogenic temperatures.[27] In the above examples, the phenomenon of chromism is not associated with disorder in the solid state of the compound under investigation and therefore differs from that in the present work.

Piroxicam is a potent, long-acting, nonsteroidal, antiinflammatory drug.[28,63] It is an enolic acid and an oxicam derivative (Figure 1).[28] While crystalline piroxicam is colorless and

contains neutral piroxicam molecules,[29,30] crystalline piroxicam monohydrate,[31] derivatives of piroxicam alkylated on the pyridyl nitrogen,[32] and 1:1 piroxicam:*β*-cyclodextrin complex[33] are all bright yellow and contain zwitterionic piroxicam molecules. The melt of piroxicam is also yellow. Metal complexes of piroxicam, in which the piroxicam molecule exists as a similar zwitterion, are also colored.[34] Solutions of piroxicam in polar solvents are also yellow and contain zwitterionic piroxicam molecules.[32,35] As compared with the neutral piroxicam molecule in Figure 1, a zwitterionic piroxicam molecule has several resonance forms arising from the anionic enolate and cationic pyridinium functional groups, as shown in Scheme 1. The yellow color of various crystalline compounds and solutions of piroxicam is attributed to extended conjugation of the zwitterionic piroxicam molecules.
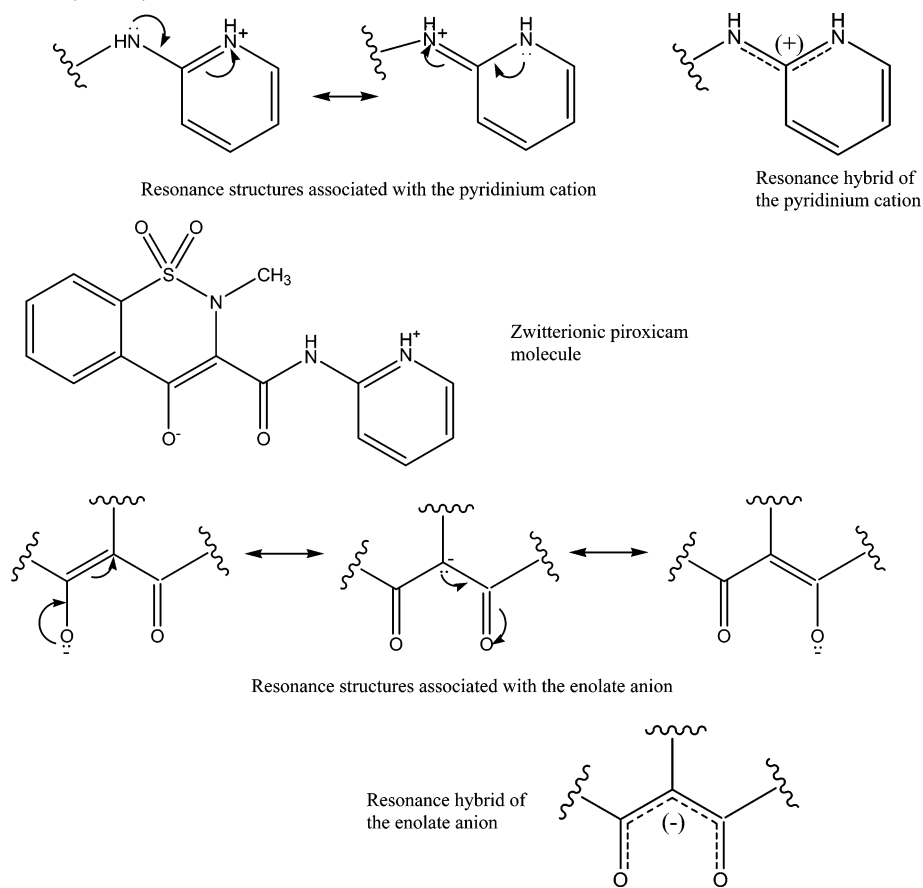
Shakhtschneider[36] reported that the *β* form of piroxicam turned yellow upon milling and that this yellow color disappeared during storage or annealing and was accompanied by recrystallization of the drug. It was suggested that, upon milling, the *β* form of piroxicam underwent a change in its molecular structure to that of the monohydrate.[36] However, this phenomenon was not investigated further. The present work provides evidence for the formation of zwitterionic piroxicam molecules in the amorphous form from neutral piroxicam molecules in the crystalline form under mechanical stress. The yellow color of amorphous piroxicam is attributed to zwitterionic piroxicam molecules, which are formed by an intermolecular proton transfer. To the best of our knowledge, the present report is the first that describes a system in which proton transfer accompanies the solid-state disorder induced by mechanochromism. Spiropyrans of the indoline series have been reported to undergo a similar mechanochromism, in addition to their photo- and thermochromic effects. However, the chromic effects are attributed to the rupture of a weak C−O bond, resulting in chemical transformation.[37]

The above phenomenon of chromism, induced by mechanical stress in organic crystals, should be distinguished from color polymorphism, which refers to polymorphism accompanied by color differences. Color polymorphism may arise from such molecular differences as hydrogen bonding (e.g., dimethyl-3,6-dichloro-2,5-dihydroxyterephthalate[38]) or conformation (e.g., 5-methyl-2-[(2-nitrophenyl)amino]-3-thiophenecarbonitrile[39]) of the molecule in the various crystal forms. Polymorphism is

(14) Heller, H. G.; Asiri, A. M. Tribochromic Compounds and their Applications. PCT Int. Appl. WO 94 26,729 (1994).
(15) Charych, D. H.; Nagy, J. O.; Spevak, W.; Bednarski, M. D. *Science* **1993**, *261*, 585.
(16) Reichert, A.; Nagy, J. O.; Spevak, W.; Charcych, D. *J. Am. Chem. Soc.* **1995**, *117*, 829−830.
(17) Charych, D.; Cheng, Q.; Reichert, A.; Kuziemko, G.; Stroh, M.; Nagy, J. O.; Spevak, W.; Stevens, R. C. *Chem. Biol.* **1996**, *3*, 113−128.
(18) Heller, H. G. In *Photochromics for the Future Electronic Materials*; Miller, L. S., Mullin, J. B., Eds.; Plenum, New York, 1991.
(19) Reichardt, C. *Solvents and Solvent Effects in Organic Chemistry*; VCH: Weinheim, Germany, 1990; pp 3, 285, 286.
(20) Rohrig, U. F.; Troppmann, U.; Frank, I. *Chem. Phys.* **2003**, *289*, 381−388.
(21) Tipikin, D. S. *Russ. J. Phys. Chem.* **2001**, *75*, 1720−1722. [Translated from *Zh. Fiz. Khim.* **2001**, *75*, 1876−1879].
(22) Nallicheri, R. A.; Rubner, M. F. *Macromolecules* **1991**, *24*, 517−525.
(23) Tomioka, Y.; Tanaka, N.; Imazeki, S. *J. Chem. Phys.* **1989**, *91*, 5694−5700.
(24) Frank, I.; Grimme, S.; Peyerimhoff, S. D. *J. Phys. Chem.* **1996**, *100*, 16187−16194.
(25) Cohen, M. D.; Schmidt, G. M. J. *J. Phys. Chem.* **1962**, *66*, 2442−2446; Inabe, T.; Okinawa, K.; Okamoto, H.; Mitani, T.; Murayama, Y.; Takeda, S. *Mol. Cryst. Liq. Cryst.* **1992**, *216*, 229.
(26) Reetz, M. T.; Hoger, S.; Harms, K. *Angew. Chem., Int. Ed. Engl.* **1994**, *33*, 181−183.
(27) Benedict, C.; Langer, U.; Limbach, H. H.; Ogata, H.; Takeda, S. *Ber. Bunsen-Ges. Phys. Chem.* **1998**, *102*, 335−339.
(28) Majerus, P. W.; Broze, G. J.; Miletich, J. P.; Tollefsen, D. M. In *Goodman and Gilman's The Pharmacological Basis of Therapeutics*, 9th ed.; Hardman, J. G.; Limbird, L. E., Eds.; New York: McGraw-Hill: New York, 1996; pp 640−641; *The Merck Index*, 13th ed.; Merck & Co., Inc.: Whitehouse Station, NJ; 2001; p 7588.

(29) Kojic-Prodic, B.; Ruzic-Toros, Z. *Acta Crystallogr.* **1982**, *B*38, 2948−2951.
(30) Vrecer, F.; Vrbinc, M.; Meden, A. *Int. J. Pharm.* **2003**, *256*, 3−15.
(31) Reck, G.; Dietz, G.; Laban, G.; Gunther, W.; Bannier, G.; Hohne, E. *Pharmazie* **1988**, *43*, 477−481.
(32) Bordner, J.; Hammen, P. D.; Whipple, E. B. *J. Am. Chem. Soc.* **1989**, *111*, 6572−6578; Hammen, P. D.; Berke, H.; Bordner, J.; Braisted, A. C.; Lombardino, J. G.; Whipple, E. B. *J. Heterocycl. Chem.* **1989**, *26*, 11−16.
(33) Redenti, E.; Zanol, M.; Ventura, P.; Fronza, G.; Comotti, A.; Taddei, P.; Bertoluzza, A. *Biospectroscopy* **1999**, *5*, 243−251.
(34) Santi, E.; Torre, M. H.; Kremer, E. *Vib. Spectrosc.* **1993**, *5*, 285−293.
(35) Geckle, J. M.; Rescek, D. M.; Whipple, E. B. *Magn. Reson. Chem.* **1989**, *27*, 150−154.
(36) Shakhtschneider, T. P. *Solid State Ionics* **1997**, *101−103*, 851−856; Shakhtschneider, T. P.; Boldyrev, V. V. Mechanochemical synthesis and mechanical activation of drugs. In Boldyreva, E.; Boldyrev, V., Eds.; *Reactivity of Molecular Solids*; John Wiley & Sons: Ltd.: Chichester, 1999; pp 271−311.
(37) Tipkin, D. S. *Russ. J. Phys. Chem.* **2001**, *75*, 1720−1723.
(38) Byrn, S. R.; Curtin, D. Y.; Paul, I. C. *J. Am. Chem. Soc.* **1972**, *94*, 890−898; Yang, Q. C.; Richardson, M. F.; Dunitz, J. D. *J. Am. Chem. Soc.* **1985**, *107*, 5535−5537; Yang, Q.; Richardson, M. F.; Dunitz, J. D. *Acta Crystallogr.* **1989**, *B45*, 312−323.
(39) Yu, L.; Stephenson, G. A.; Mitchell, C. A.; Bunnell, C. A.; Snorek, S. V.; Bowyer, J. J.; Borchardt, T. B.; Stowell, J. G.; Byrn, S. R. *J. Am. Chem. Soc.* **2000**, *122*, 585−591.

Scheme 1. Zwitterionic Piroxicam Molecule Showing the Resonance Structures Associated with the Positively Charged Pyridinium (top) and Negatively Charged Enolate (bottom)

Resonance structures associated with the pyridinium cation

Resonance hybrid of the pyridinium cation

Zwitterionic piroxicam molecule

Resonance structures associated with the enolate anion

Resonance hybrid of the enolate anion

unambiguously established by solving the crystal structures of the various polymorphs. However, certain molecules may show dynamic proton tautomerism in their crystal structures.

Piroxicam has three colorless polymorphs, forms I ($\mathbf{P_I}$), II ($\mathbf{P_{II}}$), and III ($\mathbf{P_{III}}$).[40] However, the crystal and molecular structures of only two polymorphs, $\mathbf{P_I}$[29] and $\mathbf{P_{II}}$,[30] have been solved. Consequently, the present study involves only these two forms. Amorphous piroxicam, $\mathbf{P_A}$, has been prepared but is unstable.[40] The crystal structure of piroxicam monohydrate ($\mathbf{PM}$) has also been reported.[31] Although melt-quenching piroxicam produces an amorphous phase, melt-quenched piroxicam was not used in this study, because piroxicam undergoes chemical degradation upon melting.[40]

Materials and methods

Piroxicam (Sigma Chemical Company, St. Louis, MO) was found to correspond to form I by powder X-ray diffractometry (PXRD) and was used as received. $\mathbf{P_{II}}$ was prepared from $\mathbf{P_I}$ as described.[40] $\mathbf{PM}$ was prepared from either $\mathbf{P_I}$ or $\mathbf{P_{II}}$ by water-mediated solid-state conversion at 25 °C as described.[41] The identities of $\mathbf{P_I}$, $\mathbf{P_{II}}$, and $\mathbf{PM}$ were confirmed by comparing their experimental PXRD patterns with those simulated from the respective known crystal structures.[29−31] We have previously attempted to prepare amorphous piroxicam by several methods;[40] however, cryogenic grinding was found to be the only technique suitable for preparing amorphous piroxicam.[40]

Piroxicam was subjected to mechanical stress in a cryogenic impact mill (6750 Freezer/Mill, SPEX CertiPrep, Inc., Metuchen, NJ), which

leads to the X-ray amorphous form, $\mathbf{P_A}$.[40] Using high-performance liquid chromatography (HPLC)[63] and one-dimensional 800 MHz proton nuclear magnetic resonance (NMR) spectroscopy, piroxicam was found not to undergo chemical degradation upon grinding.[40] $\mathbf{P_I}$ and $\mathbf{P_{II}}$ were cryoground separately according to the reported method.[40] The effect of mechanical stress on the solid-state structure and molecular structure of crystalline piroxicam was studied by PXRD, variable-temperature solid-state ^{13}C nuclear magnetic resonance spectroscopy (SSNMR), diffuse reflectance ultraviolet−visible spectroscopy (DRUVS), and diffuse reflectance infrared Fourier transform spectroscopy (DRIFTS) according to the following general procedure: At intervals of 12, 24, 36, 48, and 60 min of grinding time (i.e. 60 min of grinding time corresponds to 120 min of total operation of the mill,[40] indicating off-periods of equal duration), the grinding vial was immediately transferred to a glovebox containing phosphorus pentoxide and a dry nitrogen purge (25 °C, ∼0% RH). Sample preparation for PXRD, DRUVS, ^{13}C SSNMR, or DRIFTS was performed in this glovebox, as described in the paragraph below and took about 5 min for each sample. The prepared sample in the sample holder was then immediately transferred to a desiccator containing phosphorus pentoxide and conveyed to the relevant instrument. For PXRD, DRUVS, and DRIFTS, the grinding vial was returned to the cryogenic mill. Use of a glovebox containing phosphorus pentoxide and a dry nitrogen purge (25 °C, ∼0% RH) prevented the entry of moisture, thereby excluding the formation of piroxicam monohydrate.

For powder X-ray diffractometry, 400 mg of $\mathbf{P_I}$ and $\mathbf{P_{II}}$ were separately cryoground for 60 min, resulting in completely X-ray amorphous $\mathbf{P}$.[40] In the glovebox, the solid sample to be analyzed was packed into a glass capillary (1 mm internal diameter, Charles Supper, Natick, MA), which was then sealed by modeling clay.[40] This procedure requires minimal sample handling and ensures that the sample is not exposed to the environment during handling, transfer, or X-ray

(40) Sheth, A. R.; Bates, S.; Muller, F. X.; Grant, D. J. W. *Cryst. Growth Des.* **2004**, *4*, 1091−1098.
(41) Sheth, A. R.; Zhou, D.; Muller, F. X.; Grant, D. J. W. *J. Pharm. Sci.* **2004**, *93*, 3013−3026.

diffractometry. Furthermore, only 5−10 mg of the sample are required. The glass capillary was then transferred to a general area detector diffraction system (GADDS) X-ray diffractometer (Siemens, Madison, WI) in a desiccator containing phosphorus pentoxide. GADDS consists of a two-dimensional detector that measures the entire cone of diffracted X-rays and has previously been utilized to assess amorphous phase formation upon cryogrinding indomethacin.[42] Each PXRD run collected data for 5 min at 25 °C. PXRD confirmed the absence of piroxicam monohydrate in cryoground piroxicam.

DRUVS[43,44] was used to study changes in the electronic structure of crystalline piroxicam, P_I and P_{II}, as a result of cryogrinding. To yield a signal proportional to concentration, the acquired spectra were transformed by the Kubelka−Munk equation:[45,46]

$$F(R_\infty) = \frac{k}{s} = \frac{(1 - R_\infty)^2}{(2R_\infty)} \tag{1}$$

where $F(R_\infty)$ is the remission function or the Kubelka−Munk function, R_∞ is the absolute reflectance of an effectively infinitely thick layer, k is its molar absorption coefficient, and s is the scattering coefficient. Reflectance values are commonly measured relative to that of a suitable white standard, for which one assumes that $k = 0$ and $R_{\infty,std} = 1$ in the spectral region of interest. Under these conditions, one determines the ratio, $R_{\infty,sample}/R_{\infty,std} = r_\infty$, so that eq 1 affords

$$F(r_\infty) = \frac{k}{s} = \frac{(1 - r_\infty)^2}{2r_\infty} \tag{2}$$

$F(R_\infty)$ and $F(r_\infty)$ depend linearly on the analyte concentration at a given wavelength under the following assumptions.[44] The solid particles in the sample are (a) of dimensions much smaller than the thickness of the layer, (b) homogeneous in content and distribution within the powder bed, (c) uniformly and randomly distributed within this layer, and (d) constitute a layer of infinite thickness. Finely powdered samples fulfill this requirement in depths of 2−5 mm, or greater.[43,47]

The capacity of the DRUVS sample holder, the need for triplicate experiments, and characteristics of the powders required the starting weights of P_I and P_{II} to be 7 and 5 g, respectively. Sample preparation for DRUVS measurements in the glovebox involved the following procedures: Samples ground for various times were poured into the black sample holder, which was square (dimension 5 cm) with a circular cavity (diameter 2 cm, depth 1 cm). This cavity was filled completely with the powder, which was lightly compressed to a depth of 8 mm using a metal cylinder of diameter 2 cm to produce a smooth and even surface of the powder bed. The above procedure was followed to ensure consistency in the depth and smoothness of surface of the powder bed in the central circular cavity of the sample holder during each measurement. The powder bed was covered by a quartz window. To ensure further that the surface of the powder bed was flush with the sample holder, the latter was inverted and lightly tapped until no space remained between the quartz window and the surface of the powder bed. Furthermore, because the samples consisted of a single component (piroxicam) and were ground, the solid particles may be assumed to be homogeneous and randomly distributed within the powder bed. The above method ensured that the assumptions of the Kubelka−Munk theory were satisfied.[43−47]

The DRUVS spectra were recorded using a Cary 100 Bio UV−Vis spectrophotometer running on a windows-based Cary Win UV Application (Varian, Inc., Palo Alto, CA) with a diffuse reflectance accessory (model DRA-CA-30I, Labsphere, Inc., North Sutton, NH) equipped with an 8 in.-diameter integrating sphere. DRUVS spectra of all samples were recorded and calibrated against a Spectralon standard (Labsphere, Inc., North Sutton, NH). DRUVS readings are presented as mean ± sd ($n = 3$) and included readings of unground P_I and P_{II} at $t = 0$.

For variable-temperature ^{13}C SSNMR spectroscopy, about 400 mg of P_I and P_{II} were separately cryoground for 60 min, resulting in completely amorphous piroxicam. Sample preparation for SSNMR spectroscopy in the glovebox involved packing into 7.5-mm zirconia rotors and sealing with Kel-F endcaps. ^{13}C SSNMR spectroscopy was performed at 180 K using Chemagnetics CMX-300 spectrometers (Varian, Inc., Fort Collins, CO) operating at 75 MHz and Chemagnetics probes (Varian, Inc., Fort Collins, CO) equipped with PENCIL spinning modules. The spectra of P_I, P_{II}, and PM were acquired at room temperature; those of P_{AI} and P_{AII} were acquired at 180 K to avoid recrystallization during data collection. The probe temperature scale was calibrated using the ^{207}Pb resonance of lead nitrate, which is known to have a large temperature dependence.[48] The pulse sequence utilized to acquire all spectra employed variable-amplitude cross polarization[49] and total sideband suppression (TOSS).[50] Magic-angle spinning (MAS) was performed at 3.5−5 kHz together with a high-power ^1H decoupling field of approximately 60 kHz.[51] The spectrum of P_I was acquired using a 30-s pulse delay, a cross polarization (CP) contact time of 5 ms, and ^1H 90° pulse of 4.2 μs. A total of 2048 transients were acquired with 1024 data points, zero-filled to 8192 points. The spectrum of P_{II} was acquired using a 15-s pulse delay, 5 ms CP contact time, and a ^1H 90° pulse of 4.4 μs. A total of 4096 transients were acquired with 1024 data points, zero-filled to 8192 points. The spectrum of PM was acquired using a 7-s pulse delay, CP contact time of 2 ms, and a 4.2-μs ^1H 90° pulse. A total of 8192 transients were acquired with 1024 data points, zero-filled to 8192 points. Spectra of P_{AI} and P_{AII} were acquired using a 5-ms contact time, a 2-s pulse delay, and a ^1H 90° pulse of 4.4 μs. A total of 1024 transients were acquired for each spectrum with 256 data points filled to 2048 points. Variable contact time experiments performed on cryoground samples of P_I and P_{II} used contact times of 0.1, 0.5, 0.8, 1, 2, 3, 4, 5, 10, and 15 ms, with 256 transients acquired at each contact time. All spectra were referenced externally to the methyl peak of hexamethylbenzene at 17.35 ppm.

DRIFTS provided information about the molecular change accompanying grinding of piroxicam. Sample preparation for DRIFTS in the glovebox involved the following procedures. Samples ground for various time periods were poured into the DRIFTS sample holder. The powder surface was leveled with a spatula. The diffuse reflectance spectra of the samples were recorded using a FTIR spectrophotometer (Nicolet Magna-IR Series II, Nicolet Instrument Corp., Madison, WI) equipped with a liquid nitrogen-cooled deuterated triglycine sulfate detector and Windows-based software (OMNIC version 6.1a, Nicolet Instrument Corp., Madison, WI) for data collection and analysis. The sample holders were introduced into the DRIFTS chamber, which was continuously purged with filtered, dry air. The spectra were recorded 5 min after introduction of the sample holder to purge the chamber of residual moisture, carbon dioxide, and other contaminants that may have entered the DRIFTS chamber. Completion of purging was judged

(42) Crowley, K. J.; Zografi, G. *J. Pharm. Sci.* **2002**, *91*, 492−507.
(43) Kortum, G. *Reflectance Spectroscopy. Principles, Methods, Applications*; Springer-Verlag: Berlin, 1969.
(44) Wendlandt, W. W. M.; Hecht, H. G. *Reflectance Spectroscopy*; Interscience Publishers: New York, 1966.
(45) Kubelka, P.; Munk, F. *Z. Technol. Phys.* **1931**, *12*, 593−601.
(46) Kubelka, P. *J. Opt. Soc. Am.* **1947**, *38*, 448−457.
(47) Brittain, H. G. Ultraviolet/Visible diffuse reflectance spectroscopy. In: Brittain, H. G., Ed.; *Physical Characterization of Pharmaceutical Solids*; Marcel Dekker: New York, 1995; pp 37−58.

(48) Bielecki, A.; Burum, D. P. *J. Magn. Reson., Ser. A* **1995**, *116*(2), 215−220; Ferguson, D. B.; Haw, J. F. *Anal. Chem.* **1995**, *67*, 3342−3348; Takahashi, T.; Kawashima, H.; Sugisawa, H.; Baba, T. *Solid State Nucl. Magn. Reson.* **1999**, *15*, 119−123; Mildner, T.; Ernst, H.; Freude, D. *Solid State Nucl. Magn. Reson.* **1995**, *5*, 269−271.
(49) Pines, A.; Gibby, M. G.; Waugh, J. S. *J. Chem. Phys.* **1973**, *59*, 569−590; Peersen, O. B.; Wu, X.; Smith, S. O. *J. Magn. Reson., Ser. A* **1994**, *106*, 127−131.
(50) Dixon, W. T.; Schaefer, J.; Secfcik, M. D.; Stejskal, E. O.; McKay, R. A. *J. Magn. Reson.* **1982**, *49*, 341−345.
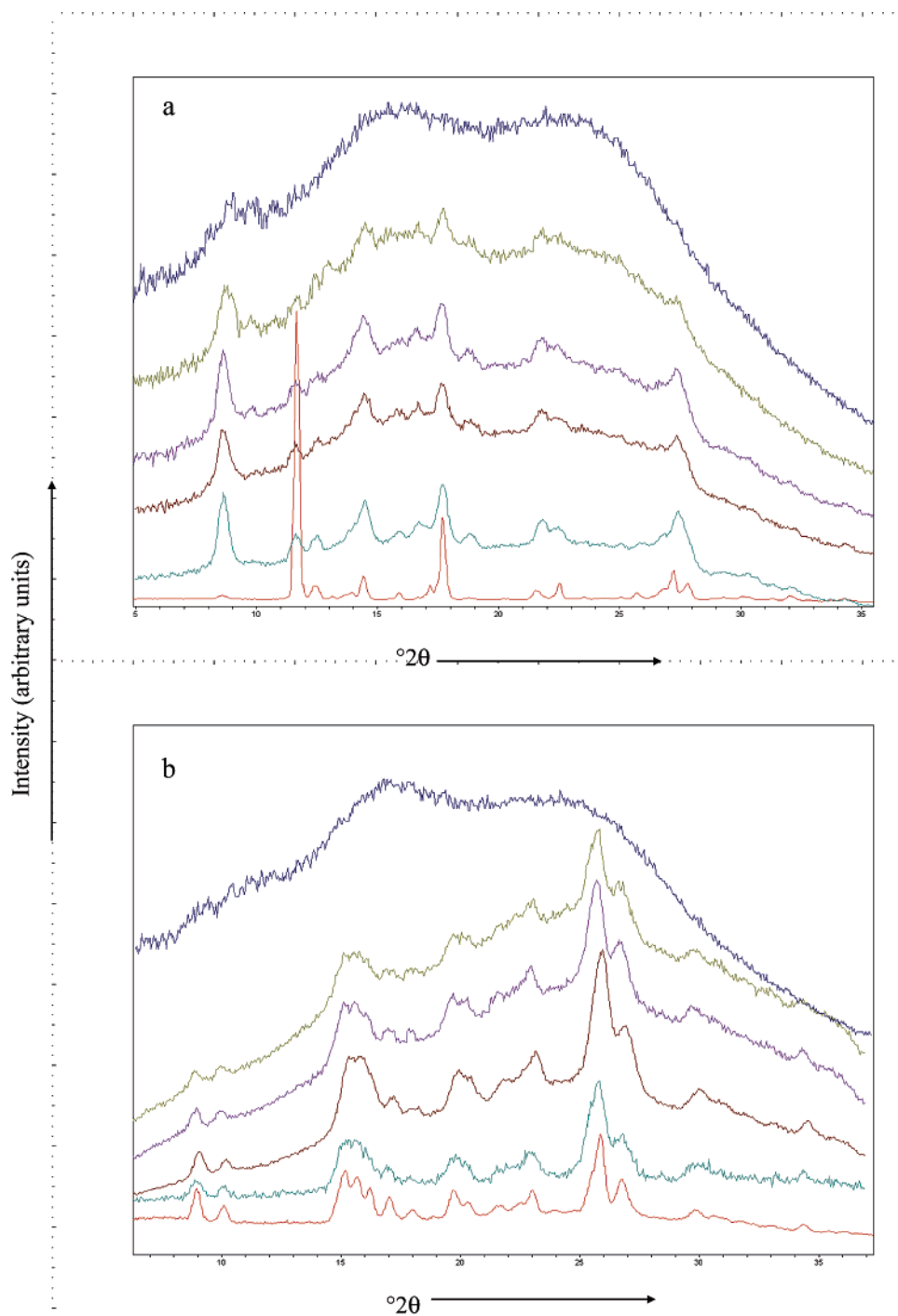(51) Stejskal, E. O.; Schaefer, J.; Waugh, J. S *J. Magn. Reson.* **1977**, *28*, 105−112.

Figure 2. Powder X-ray diffraction (PXRD) patterns of the solids starting with piroxicam Form I (a, top, lowest pattern, P_I), and starting with Form II (b, bottom, lowest pattern, P_{II}) after cryogrinding each solid for 0, 12, 24, 36, 48, and 60 min (successively stacked from bottom to top in each figure).

by disappearance of the asymmetric C=O stretch of CO_2 near 2350 cm^{-1}. For each sample, 128 scans were averaged over the wavenumber range 4000−650 cm^{-1} at a resolution of 4 cm^{-1}. All spectra were recorded against a potassium bromide blank (FTIR grade, Aldrich Chemical Co., Milwaukee, WI). At each time point, two spectra were acquired. DRIFTS spectra of unground P_I and P_{II} were also recorded at $t = 0$.

Results and Discussion

The change in crystallinity of P_I and P_{II} when cryoground for 0, 12, 24, 36, 48, and 60 min is shown in Figure 2a and b, respectively. For both polymorphs crystallinity decreases as

grinding time increases. After 60 min of cryogrinding, X-ray amorphous piroxicam is obtained. Polymorphic transformation due to grinding is not observed with either polymorph. In this contribution, completely X-ray amorphous piroxicam obtained by cryogrinding P_I for 60 min is referred to as P_{AI}, and that obtained by cryogrinding P_{II} for 60 min is referred to as P_{AII}.

Parts a and b of Figure 3 show a linear increase in the hyperchromic effect of the visible band at about 400 nm (i.e., increase in intensity of the yellow color as quantified by the Kubelka−Munk function) with respect to time for P_I and P_{II} cryoground for 12, 24, 36, 48, and 60 min. From Figures 2 and

a

Slope = 0.16 min^{-1}

$R^2 = 0.9931$

F(r_∞)

Grinding time (min)

b

Slope = 0.13 min^{-1}

$R^2 = 0.9965$
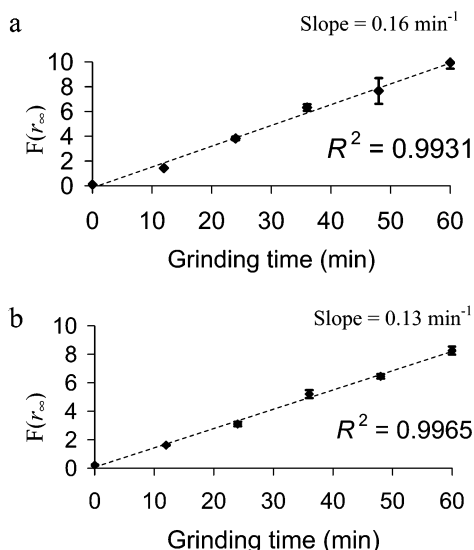
F(r_∞)

Grinding time (min)

Figure 3. Kubelka−Munk function, $F(r_\infty)$ in diffuse-reflectance ultraviolet−visible spectroscopy (DRUVS), versus grinding time of the solids starting with polymorph I (a, top, $\mathbf{P_I}$), and starting with polymorph II (b, bottom, $\mathbf{P_{II}}$), showing linear increases in intensity of the yellow color in proceeding from the crystalline to the amorphous phase during cryogrinding for increasing times. Data are expressed as mean ± sd ($n = 3$)

3, we conclude that the decrease in crystallinity of $\mathbf{P_I}$ and $\mathbf{P_{II}}$ as a result of mechanical stress is accompanied by an increase in the intensity of the yellow color with respect to grinding time. In other words, as the solid state of piroxicam changes from ordered (crystalline) to disordered (amorphous), the molecules of piroxicam undergo a structural change. In Figure 3, the data points at $t = 0$ correspond to crystalline (i.e., as-is or unground) $\mathbf{P_I}$ and $\mathbf{P_{II}}$. The crystalline solid state is evident from the PXRD pattern corresponding to $t = 0$ in Figure 2. We note here that piroxicam at $t = 60$ in the PXRD experiment is completely X-ray amorphous ($\mathbf{P_{AI}}$ and $\mathbf{P_{AII}}$, Figure 2) whereas that at $t = 60$ in the DRUVS experiment exhibited some crystallinity of the respective starting polymorph. This difference in crystallinity arises from the difference in weights of piroxicam used in the PXRD and DRUVS experiments. Although DRUVS was not performed for milling times longer than 60 min, reflectance values are expected to reach saturation. Furthermore, the presence of this residual crystallinity implies the presence of seeds of the respective starting polymorph, which could, in turn, direct recrystallization to that polymorph. Indeed, when cryo-ground piroxicam obtained at the end of the DRUVS experiment was stored at 25 °C and 0% RH over phosphorus pentoxide, recrystallization to the respective starting polymorph was observed by PXRD and was accompanied by a color change from yellow to colorless. Parts a and b of Figure 4 show the decrease in intensity of the yellow color upon storage for several days, which accompanies recrystallization to the respective starting polymorph. Figures 3 and 4 show that the kinetics of the reverse reaction recrystallization are more complicated than those of the forward reaction (crystalline to amorphous), which is characterized by a linear increase in the intensity of color with respect to time. The data in Figure 4 were found not to obey any of the 16 solid-state reaction models[52] to which they were fitted.

(52) Garner, W. E. *Chemistry of the Solid State*; Academic Press: New York,-1955; Byrn, S. R.; Pfeiffer, R. R.; Stowell, J. G. *Solid-State Chemistry of Drugs*, 2nd ed.; SSCI, Inc.:West Lafayette, IN, 1999; pp 443−460.
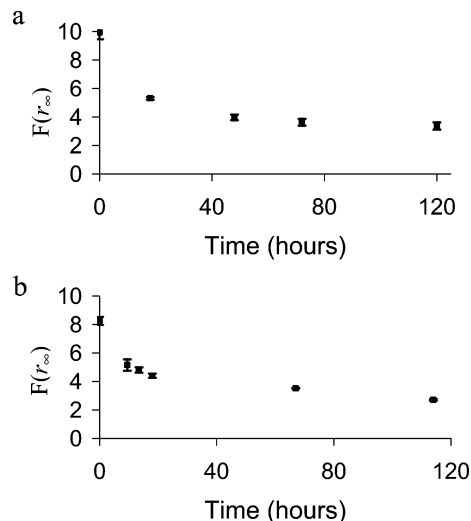
a

F(r_∞)

Time (hours)

b

F(r_∞)

Time (hours)

Figure 4. Kubelka−Munk function, $F(r_\infty)$ in diffuse-reflectance ultraviolet−visible spectroscopy (DRUVS), versus storage time showing decreases in intensity of the yellow color accompanying the recrystallization process, amorphous to crystalline, starting with the amorphous form prepared from polymorph I (a, top, $\mathbf{P_{AI}}$), and starting with the amorphous form prepared from polymorph II (b, bottom, $\mathbf{P_{AII}}$). Data are expressed as mean ± sd ($n = 3$).

From the data in the preceding paragraphs, we conclude that mechanical stress causes crystalline piroxicam to become amorphous (i.e., to amorphize). A white-to-yellow color change accompanies this phase transformation. The above change in phase and color is reversible and may be termed mechano-chromism of piroxicam.

The phase transformation, crystalline to amorphous, in piroxicam occurs when the free energy of the crystal is raised above that of the amorphous phase.[42] The following four theories have been proposed to explain this mechanism. (1) Mechanical impact produces mechanical energy that could cause local melting as a result of local increases in temperature beyond the melting point of the sample being ground.[66] (2) The Lindemann criteria suggest that pressure-induced lattice instability arises when the root-mean-square thermal displacement of the constituent atoms of a crystal lattice reaches a critical fraction of the interatomic spacing.[53] (3) Mechanical instability results in softening of the lattice vibrations. Such softening, above a critical pressure, leads to Born instability[54] and lattice collapse. (4) The spontaneous production of lattice defects upon mechanical stress raises the energy of the system, thereby providing a thermodynamic driving force, which leads to amorphization.[55,56] The melting point of piroxicam polymorphs is about 200 °C, and because milling was performed at 77 K in a bath of boiling liquid nitrogen, amorphization of piroxicam is unlikely to occur on quench-cooling of melts produced by local increases in temperature. Such a phenomenon underscores the importance of controlling the temperature during milling experiments. It has also been reported that Lindemann-type instability is an unlikely mechanism for pressure-induced amorphization.[57,58] Thus, amorphization of piroxicam under mechanical stress is preferably explained by mechanisms 3 or 4.

(53) Lindemann, F. A. *Z. Phys.* **1910**, *11*, 609−612.
(54) Born, M.; Huang, K. *Dynamical Theory of Crystal Lattices*; Clarendon: Oxford, 1954.
(55) Cahn, R. W.; Johnson, W. L. *J. Mater. Res.* **1986**, *1*, 724−732.
(56) Fecht, H. J. *Nature* **1992**, *356*, 133−135.
(57) Tse, J. S. *J. Chem. Phys.* **1992**, *96*, 5482−5487.
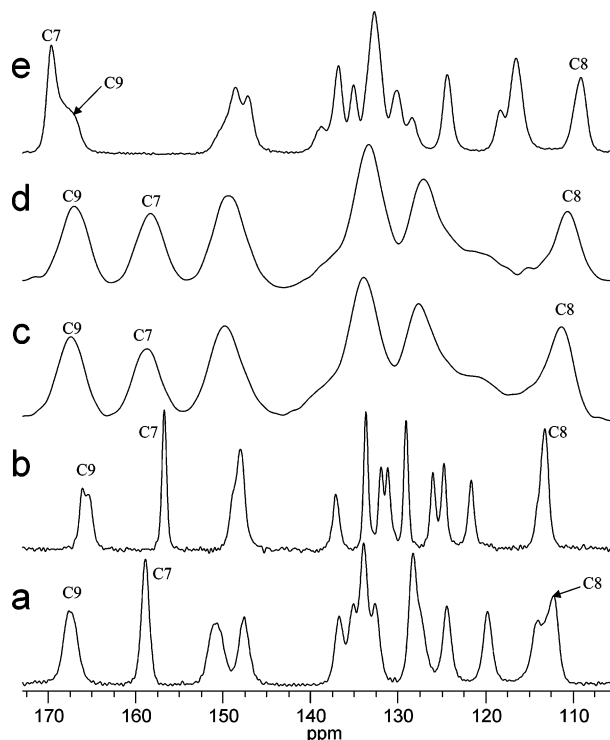(58) Tse, J. S.; Klein, M. L. *Phys. Rev. Lett.* **1987**, *58*, 1672−1675.

Figure 5. Variable-temperature ^{13}C solid-state nuclear magnetic resonance (SSNMR) spectra of piroxicam polymorph I (a, P_I), polymorph II (b, P_{II}), polymorph I which has been cryoground for 60 min to an X-ray amorphous form (c, P_{AI}), polymorph II which has been cryoground for 60 min to an X-ray amorphous form (d, P_{AII}), and piroxicam monohydrate (e, **PM**). The amorphous forms prepared by cryogrinding were handled, transferred, and packed in NMR rotors in a glovebox as described in Materials and Methods. Numbering of the carbon atoms is shown in Figure 1.

Mechanochromism of piroxicam in the solid state implies that its molecules undergo a structural change under mechanical stress. Because piroxicam was found not to undergo chemical degradation upon grinding,[40] this structural change could result from either proton transfer and/or a change in the conformation of the piroxicam molecule.

^{13}C SSNMR provides evidence of deprotonation of the acidic enol group of piroxicam molecules in P_I and P_{II} to yield a population of the enolate anion. In Figure 5 the ^{13}C SSNMR spectra of P_I, P_{II}, P_{AI}, P_{AII}, and **PM** are shown in a, b, c, d, and e, respectively. The region of the spectrum shown in Figure 5 accounts for all carbon atoms except the methyl carbon, which resonates around 40−42 ppm, depending on the solid phase of piroxicam. The discussion that follows relates specifically to the three carbon atoms of interest, C7, C8, and C9, where changes in the SSNMR spectra provide evidence of deprotonation of the enol group of piroxicam. The signal for the C9 carbonyl appears at 166−168 ppm for all five solid forms of piroxicam. While P_I and P_{II} contain neutral piroxicam molecules,[29,30] in zwitterionic piroxicam molecules, such as those in **PM**, the negative charge on the enolate oxygen is delocalized through the carbonyl oxygen,[31] imparting more carbonyl-like character to the enolate carbon−oxygen bond (Scheme 1). Thus, the signal for C7, which appears at 158.9 and 156.8 ppm for P_I and P_{II}, respectively (Figure 5, a and b), is shifted downfield to 169.5 ppm for **PM** (Figure 5e), just downfield (left) of the carbonyl C9. Furthermore, because of increased electron density at C8 due to electron delocalization in zwitterionic piroxicam molecules in **PM**, the signal for C8 is shifted upfield to 109.1
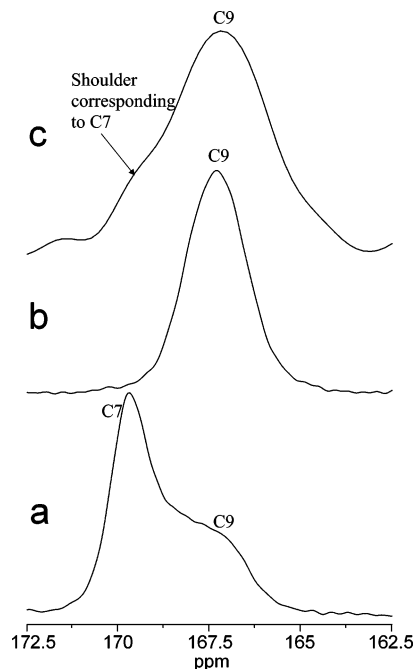

Figure 6. Variable-temperature ^{13}C solid-state nuclear magnetic resonance (SSNMR) spectra of piroxicam monohydrate (a, **PM**), piroxicam polymorph I (b, P_I), and polymorph I cryoground and packed in the NMR rotor under ambient atmospheric conditions without utilizing the glovebox (c), in the expanded spectral region 162.5−172.5 ppm. Numbering of the carbon atoms is shown in Figure 1.

ppm in **PM** (Figure 5e) from 112.3 and 113.4 ppm in P_I and P_{II}, respectively (Figure 5, a and b).

Deprotonation of the enol in P_I and P_{II} due to cryogrinding would be expected to give rise to a SSNMR signal at about 169−170 ppm, where the C7 enolate signal of **PM** resides. In the case of P_{AI} and P_{AII} such a peak is not readily visible in Figure 5, c and d, respectively. In Figure 6, a, b, and c show the respective SSNMR spectra of **PM**, P_I, and form I (cryoground and packed in the NMR rotor at ambient atmospheric conditions without utilizing the glovebox) expanded in the spectral region 162.5−172.5 ppm. In Figure 6c, the signal corresponding to the enolate is visible as a shoulder at 169.5 ppm. Amorphous piroxicam is unstable even under ambient conditions;[40] thus, packing under ambient atmospheric conditions without the aid of the glovebox increases the mobility of the amorphous phase and permits some ordering of the molecules without inducing crystallization. The lines in the spectrum of this exposed amorphous sample (Figure 6c) are ~40−50 Hz narrower than those in P_{AI} and P_{AII} (Figure 5, c and d, respectively), which were packed in the glovebox as outlined under Materials and Methods. These narrower lines permit partial resolution of this shoulder, which disappears upon recrystallization of this exposed amorphous sample. The appearance of this shoulder is evidence for the formation of deprotonated molecules of piroxicam, as deprotonation changes the chemical shift of C7 downfield to about the same chemical shift as that of C9. Presumably, this shoulder is masked in the SSNMR spectra of P_{AI} and P_{AII} by the increase in line width resulting from formation of the amorphous phase, which would smooth out such a peak. In addition to this line broadening, the similar chemical shifts of the C9 carbonyl and of the deprotonated C7 enolate would also serve to mask such a shoulder. Reduction of the integrated peak area of C7 (at 158.6 ppm)

Table 1. Integrated Peak Area of Uncharged C7 at ~159 ppm Relative to (C9 + charged C7) at ~167 ppm normalized to 100%, for Piroxicam Polymorph I (P_I), Polymorph II (P_{II}), Polymorph I Which Has Been Cryoground for 60 min to an X-ray Amorphous Form (P_{AI}), Polymorph II Which Has Been Cryoground for 60 min to an X-ray Amorphous Form (P_{AII}), and P_{AII} that Had Been Allowed to Recrystallize for Two Weeks after Cryogrinding[a]

piroxicam sample	integrated peak area of C9 (~167 ppm)	integrated peak area of C7 (~159 ppm)
P_I	100	99.8
P_{II}	100	100
P_{AI}	100	87.2
P_{AII}	100	85.6
P_{AII}, two weeks after cryogrinding	100	97.6

[a] The percentage of charged amorphous piroxicam, x, is given by the following equation:

$$\frac{x + 100}{100 - x} = \frac{100}{(\text{peak area of C7})}$$

relative to that of C9 (at 167.5 ppm) in the spectra of P_{AI} and P_{AII} provides further evidence that some molecules of the protonated C7 enol are being deprotonated by grinding. In calculating peak areas in each of spectra a, b, c, and d of Figure 5, the integrated area of the C9 peak was normalized to 100%, and the area of the C7 enol peak was calculated relative to the normalized peak (Table 1). P_I and P_{II} showed essentially identical peak areas for C9 and C7. However, amorphization of the polymorphs by cryogrinding reduces the relative peak area of the C7 enol peak to about 85%. The relative integrated peak area of P_{AII} after two weeks increased to 97.6%, indicating recrystallization accompanied by formation of the neutral enol from the charged enolate. Although amorphous piroxicam prepared by the melt-quenching technique was not studied further because of chemical degradation of piroxicam upon melting,[40] melt-quenched piroxicam also showed a reduction of the integrated peak area of C7 relative to C9. A study performed at 10 different contact times ranging from 0.1 to 15 ms for P_{AI} and P_{AII} ensured that the reduction in peak area did not result from differing cross polarization rates between carbons of interest in the crystalline and amorphous forms. The change in the relative peak areas of the C9 and C7 peaks in proceeding from crystalline (P_I and P_{II}) to amorphous (P_{AI} and P_{AII}) piroxicam could arise from dynamic broadening due to the difference in temperature, at which the spectra of P_I and P_{II} (room temperature) and P_{AI} and P_{AII} (180 K) were acquired. However, in the spectra of melt-quenched amorphous piroxicam (data not shown), which were acquired at room temperature, the ratio of the integrated peak areas of C9 and C7 is again approximately 100:84, ruling out the possibility of dynamic broadening effects. This change in the relative peak areas of the C9 and C7 peaks from 100:100 in P_I and P_{II} to about 100:85 in P_{AI} and P_{AII} indicates that the C7 signal of some of the piroxicam molecules is shifting to about 169 ppm as a result of deprotonation of the C7 enol. Deprotonation of the enol makes C7 more carbonyl-like corresponding to a downfield shift to the same spectral region where the amide carbonyl resonates (as in the case of **PM**). The ability to quantify the fractions of the neutral and charged molecules of piroxicam reported in this work is unique. We also note that the signal for C8 in the SSNMR spectra of P_{AI} and P_{AII} shifts upfield to 111.4 ppm, as is evident in Figure 5, c and d, respectively, suggesting electron

delocalization from the enolate oxygen through the carbonyl oxygen, as in zwitterionic molecules of **PM**. Such electron delocalization arising from deprotonation of the enol would increase the electron density at C8 in deprotonated molecules of piroxicam in the amorphous phase, causing increased shielding and an upfield shift.

The SSNMR shoulder at 169.5 ppm and the reduction in relative peak area of the C7 signal from 100 to 85% suggests that a relatively small population of the deprotonated species is formed in amorphous piroxicam due to cryogrinding of crystalline piroxicam. Thus, most of the amorphous piroxicam consists of neutral piroxicam molecules; the deprotonated species comprise only about 8% of the amorphous phase. A small population of charged species would be sufficient, however, to impart color to a previously colorless sample. Thus, although the intensity of the yellow color was found to increase with time of grinding, the yellow color of P_{AI} and P_{AII} was not as bright as that of crystalline **PM**, which consists entirely of zwitterionic piroxicam molecules.

DRIFTS provides evidence of protonation of the pyridine N during cryogrinding. While variable-temperature ^{15}N SSNMR spectroscopy could also be performed to detect protonated pyridinium species,[65] the seemingly low population, as detected by ^{13}C SSNMR spectroscopy in this work, would make analysis for natural abundance ^{15}N studies prohibitively long. Curves a, b, c, and d of Figure 7 show the DRIFTS spectra in the fundamental region of P_I, P_{II}, P_{AI}, and P_{AII}, respectively. The peaks at 3340 (curve a, Figure 7) and 3393 cm^{-1} (curve b, Figure 7) correspond to the N−H stretch in P_I and P_{II}, respectively, as expected for hydrogen-bonded trans secondary amides.[59] Appearance of the N−H stretch for P_{II} at a higher frequency than that for P_I can be explained as follows. In P_{II}, the N−H group is involved in a single intramolecular hydrogen bond (Figure 8b), whereas in P_I, it participates in a bifurcated hydrogen bond (Figure 8a). Thus, the N−H bond in P_{II} is shorter with a higher force constant, resulting in its infrared band appearing at higher frequency. Bands corresponding to O−H absorption are absent in the fundamental region of the DRIFTS spectra, owing to the strong O−H- -O hydrogen bonds[29−31] in both polymorphs, as previously reported.[59] Presumably, the O−H stretch appears as a weak band, which is superimposed on the strong C−H stretching vibration near 3000 cm^{-1}. Given the 4 cm^{-1} resolution of the DRIFTS instrument used in this study, the band corresponding to C=O stretch for both polymorphs (1630 cm^{-1} for P_I and 1642 cm^{-1} for P_{II}) was found to remain unchanged during milling, suggesting that this carbonyl group remains intact during grinding. In Figure 7, c and d show that, while the peak corresponding to the original N−H stretch remains unchanged, a new peak in this region appears at 3383 cm^{-1} for P_{AI} and at 3344 cm^{-1} for P_{AII}. This new band in the N−H stretch region corresponds to a second N−H bond in P_{AI} and P_{AII}, suggesting protonation of the basic pyridine N. This protonation could occur only if the acidic enol were first deprotonated. In fact, the H atom of the enol is known

(59) Colthup, N. B.; Daly, L. H.; Wiberley, S. E. *Introduction to Infrared and Raman Spectroscopy*, 3rd ed.; Academic Press: New York, 1990; Socrates, G. *Infrared and Raman Characteristic Group Frequencies*, 3rd ed.; Wiley: Chichester, New York, 2001; Bellamy, L. J. *The Infrared Spectra of Complex Molecules*, 3rd ed.; Chapman and Hall Ltd.: London, UK, 1975.
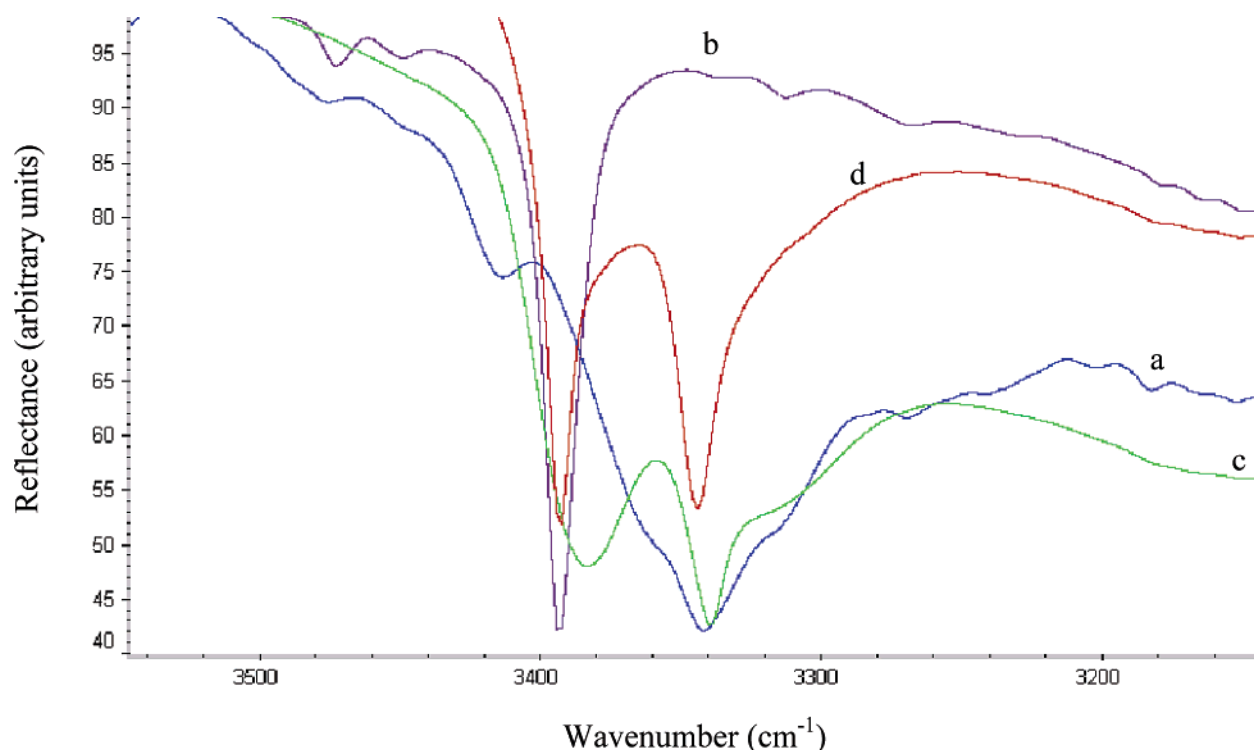
Figure 7. Diffuse-reflectance infrared Fourier transform spectroscopy (DRIFTS) curves showing N—H stretch in the fundamental region for piroxicam polymorph I (a, P_I), polymorph II (b, P_{II}), polymorph I which has been cryoground for 60 min to an X-ray amorphous form (c, P_{AI}), and polymorph II which has been cryoground for 60 min to an X-ray amorphous form (d, P_{AII}).
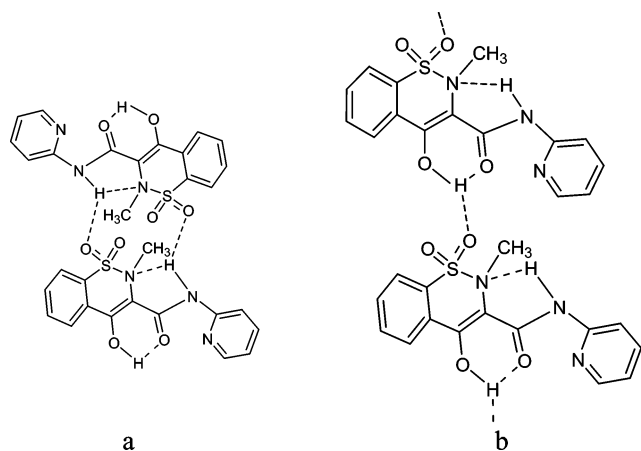

Figure 8. Hydrogen bond pattern of piroxicam form I (a, left, P_I) and form II (b, right, P_{II}).[40]

to be labile,[32] its acidity being remarkably enhanced (pK_a 1–2)[60] by the presence of the basic pyridyl group. The relative acidic strengths of the enol and pyridine groups in piroxicam have previously been discussed[32] on the basis of the hard–soft acid–base principle.[61] Due to planarity of the piroxicam molecule, the enol H and pyridine N are far apart, so that such a proton transfer is necessarily intermolecular, resulting in a charged species. As mentioned previously, DRUVS data in a and b of Figure 3 suggest that reflectance values are expected to reach saturation during longer milling times. The DRIFTS spectra, however, indicate significant amorphization due to the small

initial mass of piroxicam (about 400 mg) used for milling in the DRIFTS experiment.

We have previously reported differences between the nature of P_{AI} and P_{AII}, both of which appear to be strong glasses with a small change in heat capacity on heating.[40] During heating in DSC, T_g of P_{AII} was not observed, while that of P_{AI} was observed in two of three runs (extrapolated T_g onset 0.2 ± 0.9 °C, 273.4 ± 0.9 K),[40] but was weak. Recently, we have also described the use of pairwise distribution function transforms (PDF) of experimental PXRD data to identify the characteristic atom → atom distances (i.e., coordination numbers and nearest neighbor distances) in P_{AI} and P_{AII} and to understand the previously reported differences in their recrystallization behavior based on their local structure.[64] We note that amorphous piroxicam is isotropic overall but exhibits local anisotropy.[40,64] In other words, although this amorphous form does not possess order on a larger scale, it will be characterized by local molecular order or packing, driven by molecular shape and size anisotropy. This order or packing has typical length scales of ~20 Å in amorphous piroxicam and differs from that in any of the crystalline polymorphs. Amorphous piroxicam may therefore consist of local clusters of size ~20 Å separated by voids and dislocations. Because this local molecular packing need not be associated with long-range order, it may have a local energy that is lower than that of any of the crystalline polymorphs.

(60) Takacs-Novak, K.; Kokosi, J.; Podanyi, B.; Noszal, B.; Tsai, R.-S.; Lisa, G.; Carrupt, P.-A.; Testa, B. *Helv. Chim. Acta* **1995**, *78*, 553–562.
(61) Pearson, R. G.; Songstad, J. *J. Am. Chem. Soc.* **1967**, *89*, 1827–1836; Pearson, R. G. *J. Chem. Educ.* **1968**, *45*, 581–587.
(62) Katrusiak, A.; Katrusiak, A. *Org. Lett.* **2003**, *5*, 1903–1905.
(63) *The United States Pharmacopoeia* XXVII (USP27/NF22, 27th rev.); The United States Pharmacopoeial Convention, Inc.: Rockville, MD, 2004.
(64) Sheth, A. R.; Bates, S.; Muller, F. X.; Grant, D. J. W. *Cryst. Growth Des.* **2005**, *5*, 571–578.
(65) Lorente, P.; Shenderovich, I. G.; Golubev, N. S.; Denisov, G. S.; Buntkowsky, G.; Limbach, H.-H. *Magn. Reson. Chem.* **2001**, *39*, S18–S29.
(66) Urakaev, F. Kh.; Boldyrev, V. V. *Inorg. Mater.* **1999**, *35*, 302–305. Translated from *Neorganicheskie Mater.* **1999**, *35*, 377–381.
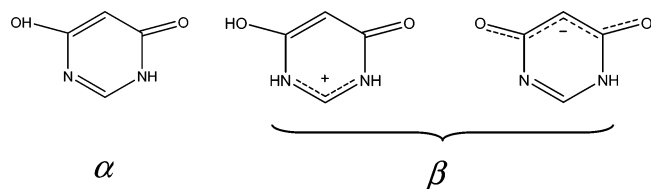(67) Wehrle, B.; Limbach, H.-H. *Chem. Phys.* **1989**, *136*, 223–247.

Figure 9. Molecular structure of 4,6-pyrimidinedione showing neutral molecules in the α polymorph, which is pale yellow, but charged molecules in the β polymorph, which has a deeper color (orange).[62] Like the structure of piroxicam shown in Figure 1, 4,6-pyrimidinedione also contains the enol and amide functions adjacent to each other. However, in 4,6-pyrimidinedione, these functions are contained in the same ring system, unlike those in piroxicam.

Figure 10. Change in the wavelength of maximum absorbance, λ_{max}, as a function of cryogenic grinding time for piroxicam forms I ($\mathbf{P_I}$) and II ($\mathbf{P_{II}}$). Data are expressed as mean $\pm$ sd ($n = 3$).

Furthermore, amorphous forms prepared by grinding, unlike those prepared from the melt, usually possess characteristics of the original polymorph, corresponding to "polymorphic memory", which would direct recrystallization to the original polymorph. $\mathbf{P_{AI}}$ and $\mathbf{P_{AII}}$ were found to possess similar short-range interactions.[64] Residual memory of $\mathbf{P_I}$ in $\mathbf{P_{AI}}$ (i.e. the presence of $\mathbf{P_I}$-like residual long-range order in $\mathbf{P_{AI}}$) explains its observed recrystallization to $\mathbf{P_I}$.[64] However, loss of polymorphic memory of $\mathbf{P_{II}}$ in $\mathbf{P_{AII}}$ (i.e. absence of $\mathbf{P_{II}}$-like residual long-range order in $\mathbf{P_{AII}}$) was found,[64] which is unusual, because amorphous forms prepared by grinding are expected to retain memory of the original polymorph. This loss of polymorphic memory appears counterintuitive and suggests that $\mathbf{P_{AII}}$ could recrystallize to a crystalline form different from the initial crystalline form.[64]

An interesting example of charged molecules giving rise to color is that of 4,6-pyrimidinedione (Figure 9), in which the polymorph containing positive and negative ions of the molecule has a deeper color (orange) than the polymorph containing neutral molecules (pale yellow).[62] 4,6-Pyrimidinedione, like piroxicam, also contains the enol and amide functions adjacent to each other. Furthermore, as mentioned in the Introduction, crystalline piroxicam monohydrate,[31] derivatives of piroxicam alkylated on the pyridyl nitrogen,[32] and 1:1 piroxicam:β-cyclodextrin complex[33] all contain zwitterionic piroxicam molecules and are bright yellow. Thus, it appears that the observed yellow color of amorphous piroxicam is a result of the ionic character of the charged species, which results from intermolecular proton transfer between neutral piroxicam molecules induced by mechanical stress. The results of ab initio calculations that provide further evidence of charged species of piroxicam, which give rise to the yellow color, will be submitted in a separate manuscript.

As a result of the charged species involved, the above transformation is expected to result in a change in the dipole moment of the molecules in the solid. Hence, the position of the peak in the DRUVS spectrum is expected to change with time of grinding, as neutral piroxicam molecules in the colorless, crystalline solid acquire charge in the yellow, amorphous solid. Figure 10 shows the change in peak position upon grinding of $\mathbf{P_I}$ and $\mathbf{P_{II}}$, respectively. For $\mathbf{P_I}$, we observe a steady hypsochromic shift with increasing grinding time, whereas for $\mathbf{P_{II}}$, we observe a bathochromic shift from $t = 0$ to $t = 12$ min, which is then followed by a hypsochromic shift. Such differences in trend are likely related to the differences between $\mathbf{P_I}$ and $\mathbf{P_{II}}$ in their mechanism of the crystalline to amorphous transformation. For example, amorphization of $\mathbf{P_I}$ may involve disordering of the piroxicam dimers and weakening of the van der Waals forces between the dimers, whereas amorphization
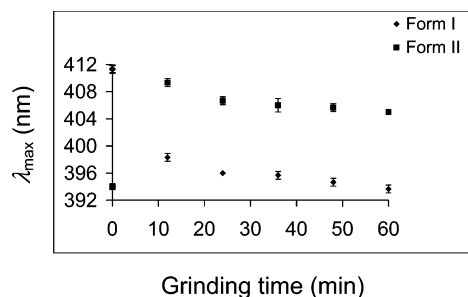
of $\mathbf{P_{II}}$ may involve breakage of the infinite hydrogen-bonded chains of piroxicam molecules. The increase in disorder of both polymorphs is accompanied by proton transfer.

Other compounds may demonstrate mechanochromism accompanied by intermolecular proton transfer and change in the solid state. For example, the nonsteroidal, antiinflammatory drug, indomethacin, (1-(4-chlorobenzoyl)-5-methoxy-2-methyl-1*H*-indole-3-acetic acid), also undergoes a color change from colorless to yellow upon grinding. Solutions of indomethacin in polar solvents are also yellow. While previous studies of this system are not detailed, the cause of the color change may be similar to that for piroxicam.

Compounds exhibiting mechanochromic behavior accompanied by a change in their solid state during grinding appear to possess hydrogen-bonding ability, which causes neutral molecules to order specifically in their crystalline state. Grinding, which disrupts hydrogen bonding, causes the molecules to disorder, such that the disordered molecules are free to undergo an intermolecular proton transfer from the acidic functional group of one molecule to the basic functional group of another, resulting in a population of charged molecules in the disordered phase. Solid phases, in which the molecule exists as a zwitterion, are also expected to be colored, as in solutions in polar or protic solvents. The amorphous phase of such molecules prepared by grinding may be unstable under ambient conditions because of the existence of disordered charged molecules, which would have a high propensity to revert to neutral, hydrogen-bonded molecules in the crystalline form, thereby reducing the free energy of the system. The intensity of color produced by grinding would depend on populations of charged species and the extent of delocalization of the π-electron system. An intermolecular proton transfer might accompany a change in the solid state of a compound under mechanical stress without a color change. The absence of such a color change would hinder identification of such a physical change. However, the instability of the resulting amorphous phase may still arise from the formation of charged molecules under mechanical stress.

Conclusions

Crystalline piroxicam, under mechanical stress, undergoes mechanochromism and transforms from the crystalline to the amorphous state. The above phase change in the solid state is accompanied by a change in molecular structure, which results in a color change from a colorless powder (white, crystalline piroxicam) to a yellow mass (amorphous piroxicam). The intensity of the yellow color increases linearly with time of application of the mechanical stress. While the solid-state change

corresponds to amorphization, the molecular change corresponds to intermolecular proton transfer between neutral piroxicam molecules in the crystalline phase. The yellow color of amorphous piroxicam is associated with the ionic character of the charged piroxicam molecules formed by intermolecular proton transfer. The charged piroxicam molecules comprise only about 8% of the amorphous phase. The reverse reaction, from amorphous (yellow) to crystalline (colorless), follows kinetics that differ from those of the forward reaction. The above changes are tautomeric, no other chemical transformation being involved.

JA045823T